

# Far-infrared spectroscopy of laser power modified MnO nanoparticles

B. BABIC<sup>a</sup>, B. HADZIC<sup>a</sup>, I. KURLISZYN-KUDELSKA<sup>b</sup>, N. PAUNOVIC<sup>a</sup>, B. VASIC<sup>a</sup>, W. D. DOBROWOLSKI<sup>b</sup>, M. ROMCEVIC<sup>a</sup>, J. TRAJIC<sup>a,\*</sup>, N. ROMCEVIC<sup>a</sup>

<sup>a</sup>*Institute of Physics, University of Belgrade, Pregrevica 118, 11080 Belgrade, Serbia*

<sup>b</sup>*Institute of Physics, Polish Academy of Science, al. Lotnikow 32/46, 02-668 Warszawa, Poland*

The influence of the locally induced laser heating on MnO nanoparticles were investigated by atomic force microscopy (AFM) and far-infrared spectroscopy (FIR) at room temperature, in the spectral region between 80 and 600 cm<sup>-1</sup>. The FIR spectra were analyzed by using Maxwell-Garnet formula, where MnO nanoparticles are modeled as a mixture of homogeneous spherical inclusions in air. Laser induced heating leads to the conversion of the part MnO nanoparticles into the MnO<sub>2</sub>, Mn<sub>3</sub>O<sub>4</sub> and MnOOH, along with possible formation of elemental Mn on the sample surface.

(Received September 3, 2018; accepted June 18, 2019)

*Keywords:* Phonons, Light absorption and reflection, Laser heating, Nanoparticle

## 1. Introduction

MnO is transitional metal oxide which crystallizes in the simple rock salt structure. It is well known that this structure has a certain number of defects, usually in the cationic sublattice, what leads to the formation of structure which can be described as an ordered Mn vacancy cubic structure with the formula Mn<sub>1-δ</sub>O, where 0 ≤ δ ≤ 0.15 [1-3].

Due to this non-stoichiometry, MnO has unique electrical, magnetic, optical and mechanical properties, characteristic for the rock salt structure [1, 2]. Recently, Hiramoto and co-workers proposed a new synthetic route which enables the control of the non-stoichiometric defects in the structure [4]. Bulk MnO acts as a p-type semiconductor and has anti-ferromagnetic properties [5]. But, the presence of impurities can significantly change the magnetic properties of the MnO [6 - 9].

The size of the particles has considerable influence on the properties of MnO. For instance, literature data shows that nanometric MnO has ferromagnetic characteristics [5]. New characteristics on nanometric scale can be explained with significant changes into the surface to volume ratio. The decreasing of the particle size increases the amount of edge atoms and, consequently, the number of unsaturated chemical bonds which, further, changes the physical and chemical properties of the material. Manganese can exist in the several oxidation states among which Mn(II) is the lowest. By different oxidation treatment, manganese can be transverse in to the different, higher, oxidation states.

Recently, we have investigated the influence of the laser induced heating of ZnO(Co) [10], Bi<sub>12</sub>GeO<sub>20</sub> [11] and MnO [12] nanoparticles, with different laser powers. It has been shown that laser induced heating leads to creation of new phases, depending on laser power.

In order to further investigate the influence of the locally induced laser heating on MnO nanoparticles, non-irradiated, as well as irradiated MnO sample, were investigated by using far-infrared spectroscopy (FIR) and atomic force microscopy (AFM).

## 2. Sample characterization

Commercially available polycrystalline MnO powder of the analytical grade (Sigma-Aldrich Co) was pressed into a pellet. Verdi G optically pumped semiconductor laser with wavelength of 532 nm was used as excitation source. In this paper we analyzed one sample, at first before laser treatment and afterwards after treatment with a laser with a power of 24 mW.

AFM measurements of non-irradiated and irradiated sample with the highest energy were done using NT-MDT system NTEGRA Prima at ambient conditions. AFM images were recorded in tapping mode, using NSG01 probes from NT-MDT.

The far-infrared measurements on non-irradiated and irradiated sample with laser power (24mW) were carried out with a BOMEM DA-8 FIR spectrometer. A DTGS pyroelectric detector was used to cover the wave number range from 80 to 600 cm<sup>-1</sup>.

## 3. Results and analysis

### 3.1. AFM measurements

AFM topographies of non-irradiated (a) and irradiated (b) MnO samples are presented on Fig. 1. Fig. 1 shows a clear difference between the surfaces of the sample before and after irradiation. Prior to irradiation, a granulated structure, with well recognized grain boundaries, is visible.

Grains size is about few tens of nanometers. In our previous investigations X-ray analysis showed that mean crystallite size is about 44 nm [12] which is in good agreement with results obtained with AFM.

After irradiation, the topography of the surface was significantly changed. The grain boundaries are not visible and surface is smooth. Due to the laser induced heating and increasing of the energy, MnO particles on the surface of the samples interact with the elements and compounds from the vicinity (mostly oxygen and water) and create compounds in which manganese is in the higher oxidation state. Process is spontaneous and these different species are inhomogeneously arranged on the surface of the sample and, consequently, clear boundaries between grains are lost.

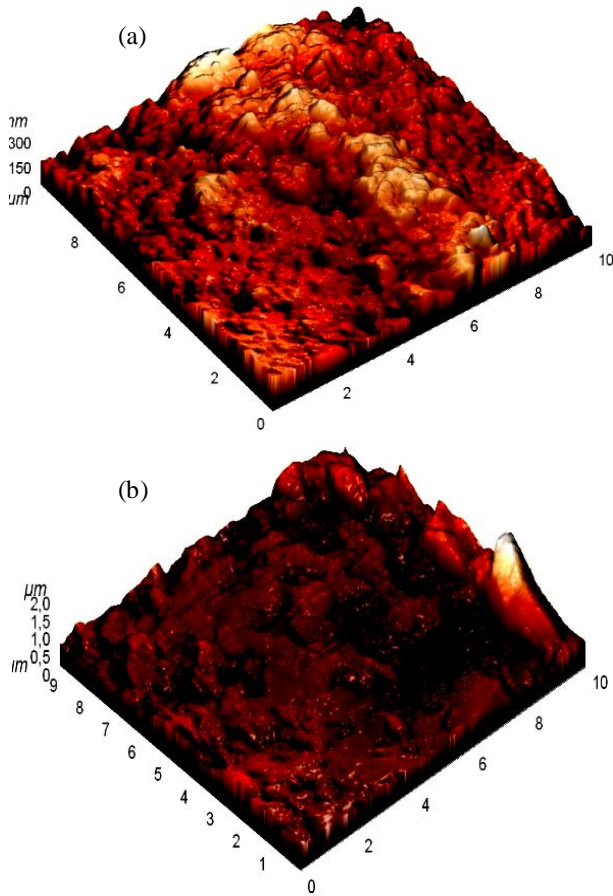


Fig. 1. AFM 3D topography of (a) non-irradiated and (b) irradiated sample of MnO nanoparticles

After irradiation, the topography of the surface was significantly changed. The grain boundaries are not visible and surface is smooth. Due to the laser induced heating and increasing of the energy, MnO particles on the surface of the samples interact with the elements and compounds from the vicinity (mostly oxygen and water) and create compounds in which manganese is in the higher oxidation state. Process is spontaneous and these different species are inhomogeneously arranged on the

surface of the sample and, consequently, clear boundaries between grains are lost.

### 3.2. Far-infrared spectroscopy

When visible light, of wavelength  $\lambda$  interacts with semiconducting nanoparticles (characteristic size  $d$ , dielectric function  $\varepsilon_2$ ) which are distributed in a medium with the dielectric constant  $\varepsilon_1$  in the limit  $\lambda \gg d$ , the heterogeneous composite can be treated as a homogeneous medium and effective medium theory is applied. There are many mixing models for the effective dielectric permittivity of such a mixture [13]. Since our samples are well defined and separated nanosized grains, we used Maxwell-Garnet model for present case. For the spherical inclusions case, the prediction of the effective permittivity of mixture  $\varepsilon_{\text{eff}}$  according to the Maxwell-Garnet mixing rule is [14]:

$$\varepsilon_{\text{eff}} = \varepsilon_1 + 3f\varepsilon_1 \frac{\varepsilon_2 - \varepsilon_1}{\varepsilon_2 + 2\varepsilon_1 - f(\varepsilon_1 - \varepsilon_2)} \quad (1)$$

Here, spheres of permittivity  $\varepsilon_2$  are located randomly in homogeneous environment  $\varepsilon_1$  and occupy a volume fraction  $f$ . The observed nanoparticles are situated in air, therefore the  $\varepsilon_1$  is 1. For dielectric function of observing nanoparticles ( $\varepsilon_2$ ) we are using the standard model [15]:

$$\varepsilon_2(\omega) = \varepsilon_\infty + \sum_{k=1}^l \frac{\varepsilon_\infty(\omega_{LOk}^2 - \omega_{TOk}^2)}{\omega_{TOk}^2 - \omega^2 - i\gamma_{TOk}\omega} - \frac{\varepsilon_\infty\omega_p^2}{\omega(\omega + i\tau^{-1})} \quad (2)$$

where  $\varepsilon_\infty$  is dielectric constant at high frequencies,  $\omega_{TOk}$  and  $\omega_{LOk}$  are transverse and longitudinal frequencies,  $\gamma_{TOk}$  is the phonon damping,  $\omega_p$  is the plasma frequency and  $\tau$  is the free carrier relaxation time. The first term in (2) is the lattice contribution whereas the second term is the Drude expression for the free carrier contribution to the dielectric constant. In this case,  $\omega_{TOk}$  is considered as characteristic frequency of the material and  $\omega_{LOk}$  is connected with the oscillator strength ( $S_k \sim \omega_{LOk}^2 - \omega_{TOk}^2$ ).

The far-infrared spectra of non-irradiated and irradiated MnO nanopowders, in the spectral range of 80 to 600  $\text{cm}^{-1}$ , at room temperature are presented in Fig. 2. The experimental data are presented by circles, while the solid lines are calculated spectra obtained by a fitting procedure based on the previously presented model. Obviously, a very good correlation between experimental data and calculated spectra is achieved. Parameters, such as: filling factors,  $f$ , plasma frequencies,  $\omega_p$ , effective permittivity of mixtures,  $\varepsilon_{\text{eff}}$ , and transversal and longitudinal frequencies  $\omega_{TO}/\omega_{LO}$ , for the non-irradiated and irradiated sample, estimated from the reflection spectra, are presented in Table 1. Induced laser heating leads to the increasing of the filling factor. Result is expected and in agreement with result obtained by AFM. Namely, phase transformation and loss of the grain boundaries leads to the decreasing of the space between particles. In accordance with that, the dielectric constant at high frequencies and plasma frequency decrease. Also, we should keep in mind that surface affected by the laser beam

is significantly smaller (radius 1 mm) in comparison with the overall surface of the pallet (radius 6 mm) which means that, in the case of the irradiation of the whole sample the differences would be more significant.

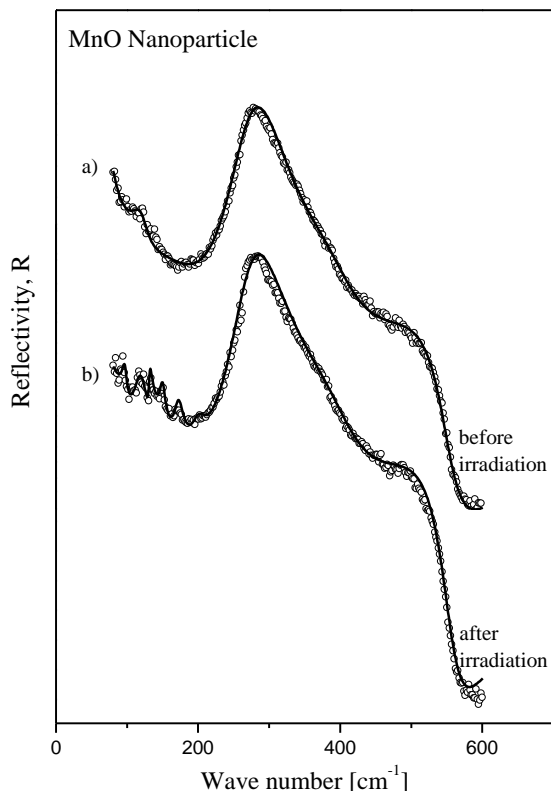


Fig. 2. Far – infrared reflection spectra of (a) non-irradiated and (b) irradiated MnO nanoparticles. The experimental data are represented by circles. The solid lines are the calculated spectra obtained by fitting procedure based on the model given by Eqs. (1,2)

Five vibration modes were determined for both non-irradiated and irradiated sample and their values are presented in Table 1. To our knowledge, there are no literature data for the FIR characterization of the MnO and we compared these results with data collected by Raman spectroscopy. By summarizing different literature data [12, 16-24], three characteristics peaks for MnO are obtained in the range 520-545, 559-595 and 645-660  $\text{cm}^{-1}$ . First two peaks we registered by using FIR spectroscopy, also. In both cases, non-irradiated and irradiated sample, additional two peaks, in the range of 310-410  $\text{cm}^{-1}$  are recorded. According to literature data, these peaks can be attributed to the  $\beta$ -MnO<sub>2</sub> (TO/LO pair at 324/330 $\text{cm}^{-1}$ ) [18, 22, 23] and  $\alpha$ -MnO<sub>2</sub> (395/405 $\text{cm}^{-1}$ ) [20, 21]. Additionally, according to Kim et al. [24] peak at 324  $\text{cm}^{-1}$  can be attributed to Mn<sub>3</sub>O<sub>4</sub>.

Additional vibration peaks that appear in FIR spectra of irradiated samples can be identified in the following way: peaks at 131, 140, 171 and 199.5  $\text{cm}^{-1}$  could be attributed to  $\alpha$ -MnOOH [20, 21] and peak at 171.5  $\text{cm}^{-1}$  could be attributed to  $\alpha$ -MnO<sub>2</sub> [20, 21].

Some authors peak at 171  $\text{cm}^{-1}$  attributed to Mn<sub>5</sub>O<sub>8</sub> phase (binary Mn<sub>2</sub><sup>2+</sup>Mn<sub>3</sub><sup>4+</sup>O<sub>8</sub> oxide with layer structure) [25]. These peaks are also registered at Raman spectra of the irradiated samples.

Table 1. Calculated fit parameters obtained from the far - infrared spectra of non - irradiated and irradiated MnO nanoparticles

	Before irradiation [ $\text{cm}^{-1}$ ]	After irradiation [ $\text{cm}^{-1}$ ]
f	0.81	0.89
$\omega_p$	301	291
$\epsilon_\infty$	2.8	2.5
$\omega_{\text{TO}}/\omega_{\text{LO}}$	120/123	116.8/117
$\omega_{\text{TO}}/\omega_{\text{LO}}$	140/148	140/140
$\omega_{\text{TO}}/\omega_{\text{LO}}$	324/330	320/330
$\omega_{\text{TO}}/\omega_{\text{LO}}$	395/405	398/407
$\omega_{\text{TO}}/\omega_{\text{LO}}$	520/526	515/558
$\omega_{\text{TO}}/\omega_{\text{LO}}$	575/590	579/584
$\omega_{\text{TO}}/\omega_{\text{LO}}$	-	96.8/97.4
$\omega_{\text{TO}}/\omega_{\text{LO}}$	-	131/131.3
$\omega_{\text{TO}}/\omega_{\text{LO}}$	-	140/141
$\omega_{\text{TO}}/\omega_{\text{LO}}$	-	171.5/172
$\omega_{\text{TO}}/\omega_{\text{LO}}$	-	199.5/200

Mode at about 100  $\text{cm}^{-1}$  (TO/LO pair is 116.8/117  $\text{cm}^{-1}$  in our case) was registered before for this group of materials [26] as a “defect mode“. Mod at 96.8/97.4  $\text{cm}^{-1}$ , in the some region, can be describe us „defect mode“, also. However, since it occurs only in an irradiated sample, we can assume that we have a case of disorder-enabled phonon (DAP) mode [27]. This is the case registered in a large number of A<sup>2</sup>B<sup>6</sup> semiconductors [28].

Finally, it was shown that FIR spectroscopy is a useful technique for the characterization of laser power induced phase changes in MnO nanoparticles.

#### 4. Conclusion

MnO nanoparticles modified by laser heating are investigated by using far-infrared spectroscopy. Effective permittivity of MnO nanoparticles (mixture of homogeneous spherical inclusions in air) are modeling by Maxwell-Garnet formula. In consequence of laser irradiation, volume fraction of nanoparticles increase while dielectric constant and plasma frequencies decrease, due to the formation of the different species on the surface of the MnO sample.

Additional vibration modes characteristic for the irradiated samples, were confirmed by using FIR method.

## Acknowledgments

This work was supported under the Agreement of Scientific Collaboration between Polish Academy of Science and Serbian Academy of Sciences and Arts. The work in Serbia was supported by Serbian Ministry of Education, Science and Technological Development (Project 45003) and in Poland by National Science Center granted under decision No. DEC-2011/01/B/ST5/06602.

## References

- [1] M. Jimenez-Melendo, A. Dominguez-Rodriguez, J. Castaing, *Acta Metallurgica et Materialia* **43**, 3589 (1995).
- [2] R. Aragon, *Physical Review B* **46**, 5328 (1992).
- [3] M. J. Radler, J. B. Cohen, G. P. Sykora, T. Mason, D. E. Ellis, J. Faber Jr., *Journal of Physics and Chemistry of Solids* **53**, 141 (1992).
- [4] M. Hiramoto, N. Okinaka, T. Akyimam, *Materials Chemistry and Physics* **134**, 98 (2012).
- [5] I. Djerdj, D. Arcon, Z. Jaglicic, M. Niederberger, *Journal of Physical Chemistry C* **111**, 3614 (2007).
- [6] N. Mironova-Ulmane, A. Kuzmin, M. Grube, *Journal of Alloys and Compounds* **480**, 97 (2009).
- [7] J. Park, E. Kang, C. J. Bae, J. G. Park, H. J. Noh, J. Y. Kim, J. H. Park, H. M. Park, T. Hyeon, *Journal of Physical Chemistry B* **108**, 13594 (2004).
- [8] A. E. Berkowitz, G. F. Rodriguez, J. I. Hong, K. An, T. Hyeon, A. Agarwal, D. J. Smith, E. E. Fullerton, *Physical Review B* **77**, 024403 (2008).
- [9] J. J. Hauser, J. V. Waszczak, *Physical Review B* **30**, 5167 (1984).
- [10] B. Hadžić, N. Romčević, D. Sibera, U. Narkiewicz, I. Kurylisyn-Kudelska, W. Dobrowolski, M. Romčević, *Journal of Physics and Chemistry of Solids* **91**, 80 (2016).
- [11] A. Kovačević, J. Ristić-Djurović, M. Lekić, B. Hadžić, G. Saleh Isa Abudagel, S. Petričević, P. Mihailović, B. Matović, D. Dramlić, Lj. Brajović, N. Romčević, *Materials Research Bulletin* **83**, 284 (2016).
- [12] B. Hadžić, B. Vasić, B. Matović, I. Kurylisyn-Kudelska, W. Dobrowolski, M. Romčević, N. Romčević, *Journal of Raman Spectroscopy* (2018) in press.
- [13] K. Karkkainen, A. Sihvola, K. Nikoskinen, *IEEE Transactions on Geoscience and Remote Sensing* **39**, 1013 (2001).
- [14] J. C. M. Garnett, *Philosophical Transactions of the Royal Society of London, Series A* **203** 385 (1904).
- [15] J. Trajic, N. Romčević, M. Romčević, V. N. Nikiforov, *Materials Research Bulletin* **42**, 2192 (2007).
- [16] F. Buciuman, F. Patcas, R. Craciun, D. R. T. Zahn, *Physical Chemistry Chemical Physics* **1**, 185 (1999).
- [17] C. Julien, M. Massot, R. Baddour-Hadjean, S. Franger, S. Bach, J. P. Pereira-Ramos, *Solid State Ionics* **159**, 345346 (2003).
- [18] C. M. Julien, M. Massot, C. Poinignon, *Spectrochimica Acta Part A* **60**, 689 (2004).
- [19] B. K. Pandey, A. K. Shahi, R. Gopal, *Materials Focus* **2**, 221 (2013).
- [20] T. Gao, H. Fjellvag, P. Norby, *Analytica Chimica Acta* **648**, 235 (2009).
- [21] S. Cheng, L. Yang, D. Chen, X. Ji, Z.-J. Jiang, D. Ding, M. Liu, *Nano Energy* **9** 161 (2014).
- [22] C. M. Julien, M. Massot, *Proceedings of the International Workshop Advanced Techniques for Energy Sources Investigation and Testing*, Sofia, Bulgaria, September 2004, pp. 1–17.
- [23] S. Kumar, A. K. Ojha, R. K. Singh, *Journal of Raman Spectroscopy* **45**, 717 (2014).
- [24] M. Kim, X. M. Chen, X. Wang, C. S. Nelson, R. Budakian, P. Abbamonte, S. L. Cooper, *Physical Review B* **84**, 174424 (2011).
- [25] J. Gao, M. A. Lowe, H.D. Abruna, *Chemistry of Materials* **23**, 3223 (2011).
- [26] H. Kepa, T. Giebultowicz, B. Buras, B. Lebech, K. Clausen, *Physica Scripta* **25(6A)**, 807 (1982).
- [27] V. Dzagan, I. Lokteva, C. Himcinschi, X. Jin, J. Kolny-Olesik, D. R. T. Zahn, *Nanoscale Research Letters* **6**, 79 (2011).
- [28] A. Ingale, K. C. Rustagi, *Physical Review B* **58**, 7197 (1998).

\*Corresponding author: jelena@ipb.ac.rs